Journal of
Biomaterials and Tissue Engineering
Vol. 3, 141–147, 2013

Molecular Dynamics Study on the Encapsulation of Prilocaine in Liposomes at Physiological pH

Giovanni Giupponi[1], María Florencia Martini[2], and Mónica Pickholz[2,*]

[1] *Departament de Fisica Fonamental, Universitat de Barcelona, Carrer Martii Franques, 08028 Barcelona, Spain*
[2] *Department of Pharmaceutical Technology, Universidad de Buenos Aires, Junin 954 RA-1053 Buenos Aires, Argentina and CONICET*

In this work, we investigated the concentration effects on the encapsulation of prilocaine (PLC), an aminoamide local anesthetic, into a small unilamellar liposome, at physiological pH. On the line of our previous work, we have carried out Molecular Dynamics (MD) simulations using a coarse grain (CG) model that allow us to reach the microsecond time scale. At physiological pH there is a partition between protonated and neutral PLCs. In order to estimate the protonated/neutral PLC ratio at physiological pH (7.4), we have used the Henderson-Hasselbach equation. We have studied three PLC:lipid molar concentrations, ranging between 10:10 to 1:4. We essentially found that all neutral PLC molecules rapidly diffuse into the hydrophobic region of the vesicle adopting an asymmetric bimodal distribution. Moreover, protonated PLC molecules partition between the external monolayer of the vesicle and the water phase, having a high rate of exchange between this two phases, with no access to the inner part of the liposome in a concentration dependent way. In this way, we found that the behavior of PLCs at physiological pH is a combination of high and low pH, especially at low concentration of local anesthetics.

Keywords: Coarse Grain, Local Anesthetics, Liposome, Molecular Dynamics, Prilocaine, Physiological pH.

RESEARCH ARTICLE

1. INTRODUCTION

The development of safer and more effective local anesthetics (LA)—pain relief drugs—has come a long way since the earliest experiments with cocaine.[1] Nowadays, a growing number of new anesthetics are used in medicine and odontology. The structure and physicochemical features of each LA determine drug potency, onset of action of sensory block and toxicity.[2] However, the relatively short duration of analgesia—due to their transfer and redistribution from the site of injection—still restricts their clinical use for the treatment of chronic pain.[3] In the last decades the development of LA drug-delivery systems made possible to manipulate some biopharmaceutical and pharmacological properties of LA, improving their therapeutic effects (long duration of action associated to low systemic toxicity) and pointing them as promising alternatives to favor the clinical use of LA agents.[4,5]

Liposomes-spherical vesicles consisting of one or more phospholipid bilayers—are currently used as effective drug carriers. For example, there are vesicle formulations for antitumor anthracyclines,[4] antifungal[5] and many others.[6,7] Liposomes are very versatile structures: their physicochemical properties can be modified by changing the types of lipids and their proportions in the liposomal formulation, the size of the vesicle, the charge of the surface (positive, negative, or neutral), the pH sensitivity, temperature sensitivity, etc.[9] In this way, liposomes can be carriers for hydrophilic or hydrophobic compounds. The size of the liposomal vesicles significantly influences drug distribution.[8,9] The encapsulation of LAs into liposomes for drug-delivery purposes has been proposed for the first time by Gesztes et al.[10] Nowadays, diverse studies have been demonstrated the clinical effectiveness of liposomal formulations containing different anesthetics.[11,12] The advantages of encapsulating LA in liposomes are the slow drug release, prolonged anesthetic effect and reduced toxicity towards the cardiovascular and central nervous systems.[4] Intensive research is focused on anesthetics trapped into liposomes, in order to enhance their activity and pharmacokinetic properties.[5]

It is important to remark that the pH of a parenteral infusion is found between 4 and 8.[13] The reason for that is related with the patient's acceptance: infused solutions of pH smaller than 3 cause pain and phlebitis, and pH greater

*Author to whom correspondence should be addressed.

than 8 cause inflammation and venous irritation. In particular, most of LAs are weak bases with pKA values between 7.5 and 8.8.[14] In this way, a partition between their charged and uncharged forms is found at physiologic pH. This partition could be quantified by the Henderson-Hasselbach equation,

$$pH = pK_a + \log \frac{[\text{neutral}]}{[\text{protonated}]} \quad (1)$$

The values between [..] represent the molar concentrations of neutral and protonated species, respectively.

The knowledge of the interaction of LA with lipids is essential in order to improve the use of liposomes as LAs drug carriers. Many techniques are used in order to elucidate these interactions.[15–17] In particular, fully atomistic molecular dynamics (MD) simulations are very powerful to study the interaction of anesthetics with model membranes, as shown for the number of articles in the literature.[15, 18–21]

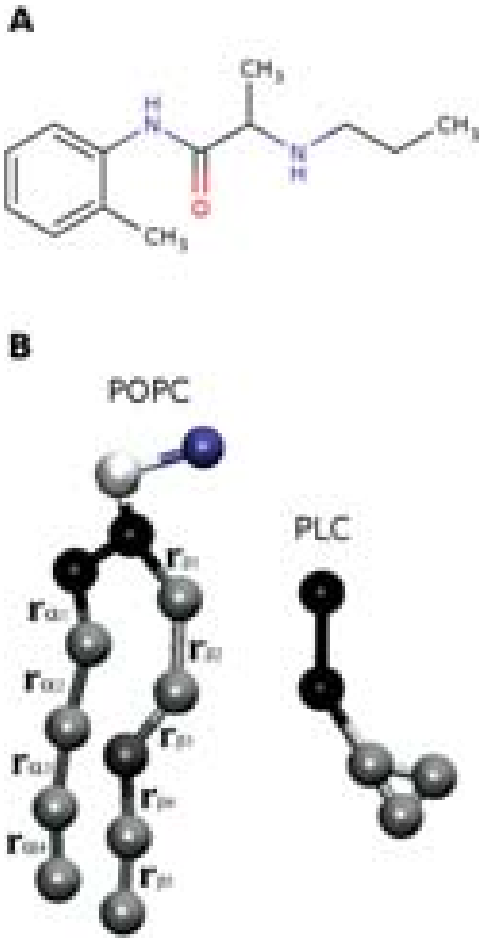

Fig. 1. (A) Chemical structure of protonated prilocaine (*p*PLC), (B) Coarse-grain representation of POPC phospholipid and PLC molecules. The ester (*E*) and the vectors of a consecutive sites of the lipid tails $\vec{r}\alpha i$ ($i = 1.4$) for the palmitoil chain, and $\vec{r}\beta j$ ($j = 1.5$) for the oleoyl chain are shown.

However, it is not possible to reach these detailed studies for big systems and long times. In this way, the use of simplified models could help us to reach important phenomena. Very recently, we have studied the encapsulation of LA prilocaine (PLC, see its chemical structure in Fig. 1(A)) into a liposome using a Coarse Grain (CG) model.[22] In this study we considered the PLCs at their neutral (high pH) and protonated (low pH) state. Regarding the importance of the formulations at physiological pH, here we extend our simulations in order to take this effect into account. At physiological pH there is a partition between neutral (*n*PLC) and protonated (*p*PLC) prilocaine molecules. The ratio of this partition was, *p*PLC/*n*PLC, was estimated as ~ 1.6, taking into account the apparent pKa of PLC in membranes is 7.6[23] and a pH of 7.4 in Henderson-Hasselbach equation (Eq. (1)). We studied three concentrations of PLC that meet this ratio. It is important to keep in mind that the protonation/deprotonation of the PLCs is a dynamical process. However, as a first approximation we consider only a fixed number of neutral and protonated species in our simulations. In next section we describe the methodology used in this study, followed by the results and conclusions.

2. METHODOLOGY

In this work, we carried out molecular dynamics simulations using a coarse grain model within the MARTINI force field[?] that can be used to investigate macromolecular phenomena at the microsecond scale.[24–30] This method aims at a systematic and portable representation for water, phospholipids, and other small molecules in terms of a few building blocks, or coarse grained (CG) particles. These CG particles interact with potential parameters optimized for use in a broad range of biomolecular applications. Four heavy atoms to one CG particle mapping rule is generally followed, and hydrogen atoms are neglected because of their small size and mass. This model considers four main types of CG particles: polar (P), nonpolar (N), apolar (C), and charged (Q). In Figure 1, we show an scheme of the CG 1-palmitoyl-2-oleoyl-sn-glycero-3-phosphatidylcholine (POPC) lipid and the CG PLC molecule, used in his work. The prilocaine molecules have been parameterized in our previous work, within this scheme.[22] The structure of the neutral PLC (*n*PLC) is essentially the same of the protonated one (*p*PLC). However, the type of CG particles and charge are different, in order to consider the charge of the protonated molecule. Besides, a chloride counterion was added in order to form a salt with *p*PLC. The rest of the CG particles for lipids, water, and ions follow the standard force field. For a detailed description of force features and parameters, see Ref. [24]. We have used the P4 model of water, instead the new developed polarizable water[31] in order to be consistent with our previous work.

In this work we study the encapsulation of a mixture of neutral and protonated PLC—in order to emulate the partition of protonated and neutral species as fisiological pH—in a POPC lipid vesicle. We considered three different concentrations that respect the 1.6 ratio:
(a) 54 *p*PLC and 34 *n*PLC,
(b) 88 *p*PLC and 55 *n*PLC, and
(c) 141 *p*PLC and 88 *n*PLC.

The chosen concentrations were thought in order to compare with our previous work:[22] the
(a) condition represents the same lipid:PLC ratio (10:1) used in the simulations of the previous work, the
(b) condition has the same amount of *p*PLC, even though in the presence of the correspondent number of *n*PLC and
(c) condition has the same amount of *n*PLC, even though in the presence of the corresponding *p*PLC.[22]

The starting point for this simulation was a preassembled POPC vesicle, containing 877 lipids (254 and 623 for the internal and external monolayer, respectively), 81550 P4 water particles. The PLCs were initially (randomly) distributed in the water phase for the case (a) (lower concentration). Besides, chloride counterions were always added randomly in the water phase, in the same concentration than *p*PLC, in order to ensure electroneutrality

The following cases were built up by addition of the extra molecules into the external water phase, starting from the equilibrated previous case. We have equilibrated the systems for 250 ns within the NPT ensemble. After equilibration, we run the system in the NVT ensemble for 1 μs.

The simulations were carried out with the GROMACS 4.0 simulation package,[32] using a simulation timestep of 40 femtoseconds with a nonbonded and electrostatic cutoff of 12 Å. The reference temperature was set to 325 K using a Berendsen thermostat with a time constant of 1.0 ps. For NPT runs, Berendsen pressure coupling was used with a reference pressure of 1 bar, time constant 5.0 ps and a compressibility of 3×10^{-5} bar^{-1}. On a computational note, we report that a fully atomistic representation of the same systems would need around a million atoms to be run with a typical simulation timestep of 2 femtoseconds. As drug diffusion and adsorption phenomena involve characteristic scales of tens of nanometers and hundreds of nanoseconds, we conclude that extensive fully atomistic simulations reaching the microsecond of such phenomena are impractical even using big supercomputers, leaving coarse grained force fields the only feasible models.

3. RESULTS

In this work, we have studied the encapsulation of three different concentrations of prilocaines, with the same *p*PLC/*n*PLC ratio: going from $\sim$1:10 (case a) to 1:4 lipid:LA ratio (case c), into a POPC lipid vesicle. Here, we discuss the main results of our study.

It is important to highlight here that most of the studied *observable* properties are converged during the NPT equilibration period. In this way, properties shown here are averaged at the stationary state of the system.

In order to have a first glance to the encapsulation mechanism, we visually check the stability of the vesicle and the diffusion of the drug. In Figure 2, we show, as an example, three snapshots that corresponding to case (a). The *n*PLC and *p*PLC are represented in green and red, respectively, and water and couterions sites were removed for visualization purpose. In this figure, the snapshot (A) corresponds to the initial configuration: the PLCs were randomly distributed in the water phase. The other two snapshots were taken at the end of the NPT equilibration run $t = 0.25$ μs and at the end of the NVT run $t = 1.25$ μs. Snapshots B and C clearly show that most of the nPLCs quickly diffused into the vesicle during the equilibration period, and remained inside during the whole simulation time, while the *p*PLC partition into both phases. Similar results were found for cases (b) and (c) (snapshots not shown).

In order to check the overall organization of the systems under study and the stability of the vesicle we computed the radial electron density profile (REDP), by time averaging the net charge $Q(r)$ (the nuclear charge corresponding to all of the atoms represented by each CG site) contained in the volume between consecutive spheres, by

$$REDP(r) \propto \left\langle \frac{Q(r)}{4/3\pi((r+\delta)^3 - r^3)} \right\rangle \qquad (2)$$

In Figure 3 we show the REDP of the 3 different systems under study: (a) 54 *p*PLC–34 *n*PLC, (b) 88 *p*PLC–55 *n*PLC, and (c) 141 *p*PLC–88 *n*PLC calculated by averaging over the 1 μs NVT simulations run. In this figure, the REDP corresponding to the POPC and water components is shown in black and blue, respectively. Comparison of the overall organization of water and vesicle and their interfaces show no noticeable difference between the three cases. In these figures, the pPLCs (in red) and nPLCs (in green) densities have been magnified 5 times for visualization purposes. We can notice that *n*PLC molecules are essentially found inside the vesicle, following a bimodal distribution for the three cases (as found in previous work[22]). By the other hand, *p*PLC molecules partitioned between the water/lipid interface of the external monolayer and the water phase, with no access to the bilayer center. Looking to the different groups (ring and tail) of the *p*PLC molecules, we find a preferential orientation of the *p*PLC molecules (results not shown), with the ring pointing to the lipid tail region and the *p*PLC tail to the the polar head groups. This fact was better described in previous publication for the low pH case, and we will not enter deeper here. On the contrary, *n*PLC does not show a preferential orientation inside the lipid membrane.

Until now, we got the qualitative idea that nPLCs are essentially found inside the vesicle and *p*PLC partition

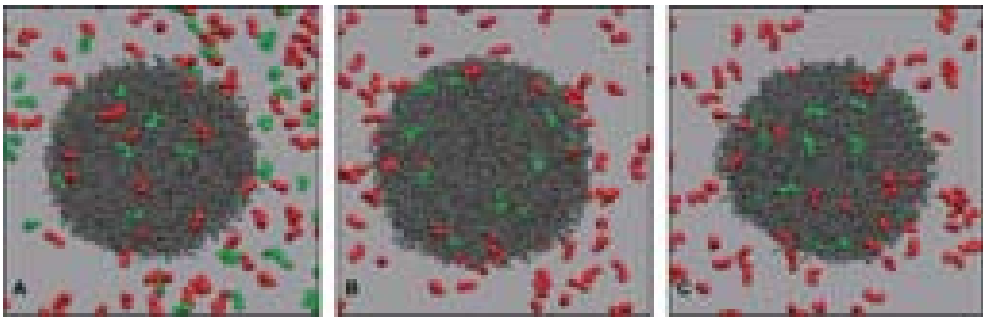

Fig. 2. Snapshots from the molecular dynamics simulations of PLC in POPC vesicles: *n*PLC in green and *p*PLC in red. The snapshots correspond to (A) the initial configuration, (B) after 250 ns of NPT run, and (C) after 1 μs of NVT run. Water and sites were removed for clarity.

between both phases. We calculate the number of PLC molecules absorbed by the vesicle as a function of time, using $\langle r \rangle = 75.0$ Å, as external vesicle radius, which is the averaged over the NVT simulation time radius. In Figures 4(A) and (B) we have separated the nPLCs and *p*PLC numbers, cases (a) in green, (b) in red and (c) in blue, respectively. We can see from Figure 4(A) that *n*PLC are essentially inside the vesicle independently on concentrations. By the other hand, in Figure 4(B) we can see an increasing number of *p*PLC inside the vesicle with the increasing of concentration. In Table I we summarized the average numbers of *n*PLC, *p*PLC and the total number of PLC encapsulated into the vesicle.

We found a little decreases of this number (from 20.7 to 19.2), when compared with the system with the same amount of *p*PLC, but in absence of *n*PLC. In this way, the presence of *n*PLC slightly diminishes the possibility of *p*PLC to get inside the vesicle.

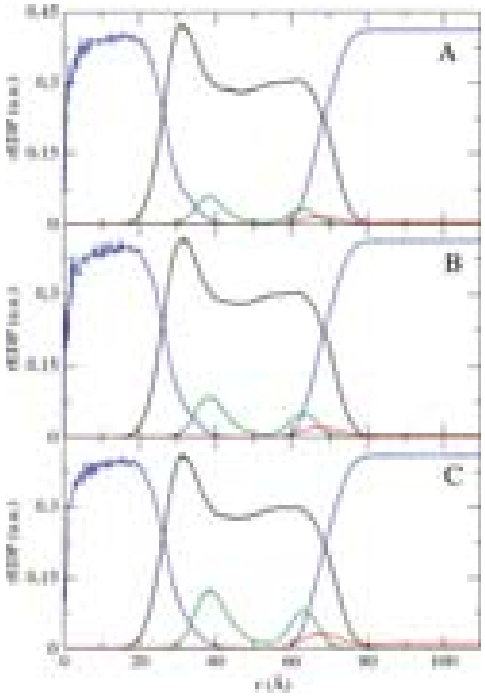

Fig. 3. Radial electron density profile (REDP) of the different components of the PLC/vesicle as a function of the r coordinate; $r = 0$ corresponds to the vesicle center. The colors are blue for water, black for POPC, green for neutral PLC, and red for protonated PLC. (A) 54 *p*PLC–34 *n*PLC, (B) 88 *p*PLC–55 *n*PLC, and (C) 141 *p*PLC–88 *n*PLC derived, from the 1 μs NVT simulations. The REDP of *n*PLC and *p*PLC were amplified 5 times for visualization purposes.

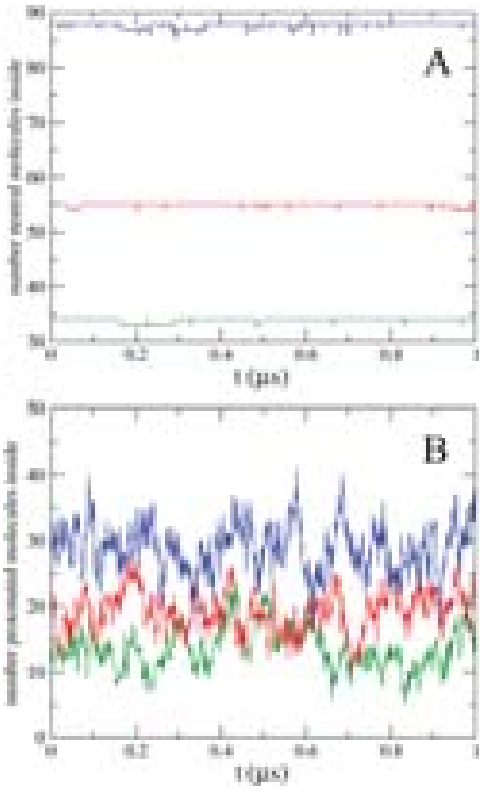

Fig. 4. Number of (A) *n*PLC and (B) *p*PLC molecules inside the vesicle as function of time for concentration *p*54*n*34 (green), *p*88*n*55 (red) and *p*141*n*88 (blue).

Table I. Number of neutral ($N_{n\text{PLC}}$), protonated prilocaine ($N_{p\text{PLC}}$) and total (N_{total}) molecules encapsulated into the vesicle.

Case	$N_{n\text{PLC}}$	$N_{p\text{PLC}}$	N_{total}
Case (a)	33.86(1)	13.6(1)	47.5
Case (b)	54.91(1)	19.2(1)	74.1
Case (c)	87.79(2)	28.9(1)	116.7

The distribution of PLCs inside the vesicle was shown in Figure 3. However, because of the spherical geometries of the system, density is difficult to visualize. In this way, we have calculated the average number of PLCs (center of mass) as function of the distance to the vesicle center. The protonated case is shown in Figure 5: (A) case (a), (B) case (b), (C) low pH case from Ref. [22] and (D) case (c). We can see from these figures that a main peak is found for the anesthetics inside the vesicle. The maxima are found essentially at a radius of $\sim$69 Å. Its position does not change with concentration but the intensity does. We can see that these peaks extend more than the 75 Å.[22] This could be explained, by the interactions of the external *p*PLC close to the surface, that interact with the lipid polar head. In this way, an effective encapsulation is found, ranging at the radius of 80 Å. However, in average, the extra encapsulation is quite low ($\sim$1–2 *p*PLC molecules). It is important to remark here that exist a fast exchange of *p*PLC between the vesicle and the aqueous phase for all the studied concentrations.[22] Besides, as found in previous work, pPLCs cannot access to the inner monolayer by diffusion.

The numbers of nPLCs (center of mass) as function of the distance to the vesicle center are shown in Figure 6: (A) case (a), (B) case (b), (C) high pH case from Ref. [22] and D-case (c). As we mention earlier, we observe two well defined peaks that correspond to the partition of *n*PLC in each of the monolayers: the inner (D_1) and outer (D_2) peaks, that correspond to the *n*PLC partitioned into the internal and external monolayer, respectively. We can see that both peaks increase with concentration, however the maxima remain at the same distance of the bilayer center ($\sim$39 Å, and $\sim$65 Å, respectively). We have calculated the number of *n*PLC partitioned in each of the monolayers. Taken into account the asymmetry of the monolayers we use as a criteria the cut radius as the middle of the gap in Figure 5(A) (54 Å) and used this difference for all the cases. Because of the asymmetry of the monolayers, it is more adequate to compare the number *n*PLC per lipid ($nPLC_{\text{lip}}$), shown in Table II. It is important to keep in mind that from the experimental point of view, it was reported in the literature a very high lipid:neutral LA ratio (3:1 or higher).[15, 17] We can see from Table II that the number of $nPLC_{\text{lip}}$ increases with concentration. Furthermore, the $nPLC_{\text{lip}}$ is higher for the inner monolayer for all the concentrations. Besides, if we compare the case (c) in which the number of *n*PLC is 88 (and 141 *p*PLC) with our earlier paper (Ref. [22]) in which only 88 *n*PLC where present, also presented in Table II, we can see that an increase of the inner $nPLC_{lip}$ (from 0.137 to 0.146) with a concomitant decrease of the outer monolayer (from 0.084 to 0.081). However these little differences are not meaningful within the error bars. By the other hand,

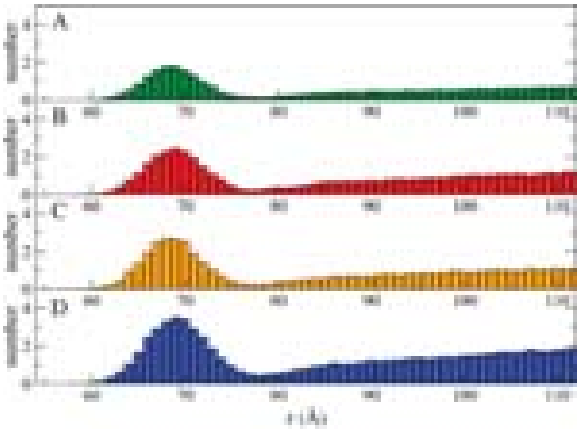

Fig. 5. Histogram of the number of protonated PLC as function of the radial distance for the different conditions: (A) case (a) in green, (B) case (b) in red, (C) 88 *p*PLC (Ref. [22]) (orange) and (D) case (c) in blue.

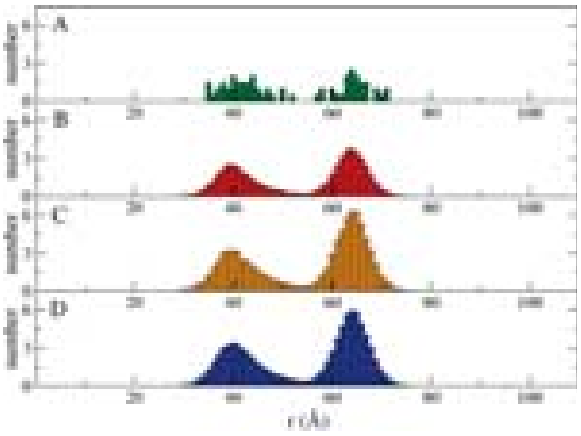

Fig. 6. Histogram of the number of neutral PLC as function of the radial distance for the different conditions: (A) case (a) in green, (B) case (b) (red), (C) 88 *n*PLC (from Ref. [22]) (orange), (D) case (c) in blue.

Table II. Number of neutral per lipid, $nPLC_{\text{lip}}$, in internal and external monolayers and ratio between the number of *n*PLC corresponding to peaks D_1 (internal monolayer) and D_2 (external monolayer), for the 3 concentrations, the same information of the system at high pH was also included.

Case	Peak D_1:$nPLC_{\text{lip}}$	Peak D_2:$nPLC_{\text{lip}}$	D_1/D_2
Case (a)	0.070(2)	0.024(1)	1.2(1)
Case (b)	0.096(4)	0.049(2)	0.8(1)
Case (c)	0.146(6)	0.081(3)	0.7(1)
Ref. [22]	0.137(6)	0.084(3)	0.7(1)

RESEARCH ARTICLE

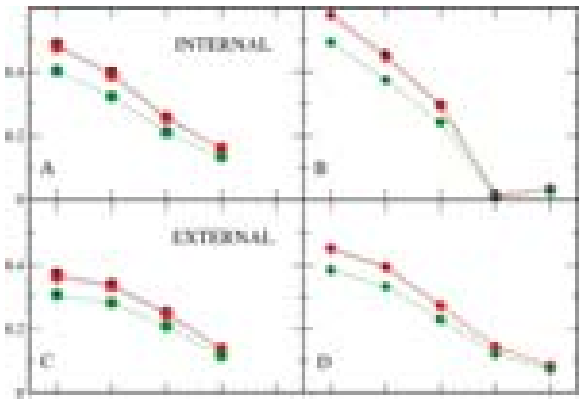

Fig. 7. Generalized order parameter of the inner (A) and (B) and outer (C) and (D) shell of the vesicle. Left pannels (A) and (C) correspond to the saturated palmitoyl chain and right pannels (B) and (D) to the insaturated oleoyl chain for the different conditions: case (a) in green, case (b) in red and case (c) in blue.

looking at the *n*PLC center of mass trajectories, we can see crossing events of these molecules between monolayers for all the studied cases. These crossing events were already reported,[1, 15, 33] here we will not enter in more details.

The effects of the solutes on the conformation of the lipid chains can be studied by monitoring the average orientation of the covalent bonds of the effective sites located in the interior of the bilayer. In this way, we have, also, studied the order parameter of the lipid tails. In this case, because of spherical symmetry of the system, we have defined the angle θ between the vectors of consecutive sites of the lipid tails and the radial versor, $\hat{r}$ and $-\hat{r}$, for the outer and inner monolayer, respectively. We have named the vectors between the consecutive CG sites as $\vec{r}_{\alpha}i$ $(i = 1, 4)$ for the palmitoil chain, and $\vec{r}_{\beta j}$ $(j = 1, 5)$ for the oleoyl chain, as shown in Figure 1(B). We have calculated the average the order parameter through the averaging of the second Legendre polynomial over all lipids and time for each of the described vectors, as

$$S = \frac{1}{2}\langle 3\cos^2\theta - 1\rangle \qquad (3)$$

In Figure 7, we show the generalized order parameter for saturated (left panels: (A) and (C)) and unsaturated (right panels: (B) and (D)) chains, for the inner (top panels) and the outer (bottom panels) shell of the liposome. As an overall view of this figure, we can notice (as expected) that the tails of the outer monolayer are more organized that inner one. The reason for that is related with the curvature and the limiting factor for the vesicle density. There is important to point out that the unsaturated tail is always more disorder that the saturated one due to the kinks of the trans-gauche conformation.[34] Respect to the concentration effects, we can see an overall organization of the lipid tails, from case (a) to case (b). However, essentially no changes of chain organization were observed between case (b) and (c).

4. CONCLUSIONS

In this work we have studied, by molecular dynamics simulations, the interaction of the local anesthetic prilocaine with small liposomes at physiological pH using a coarse grain model.[24] The use of a coarse grain model allowed us to reach relevant time and length scales of drug diffusion, otherwise impossible to observe using fully atomistic molecular dynamics. Very recently, we have studied the encapsulation process of neutral (high pH) and protonated (low pH) prilocaine in a POPC vesicle.[22] This work shed light in many aspects of the encapsulation. However, it is undoubtedly the necessity of the understanding this kind of system at physiological pH, since the pH of an infused solution should be in the range 4 to 8 to have a good patient acceptance. Moreover, the existence of the two species of PLC is needed in order to obtain the desire clinical effects: neutral molecules acts as a reservoir, while the protonated specie enhanced the exchange of the LA with the water phase. At physiological pH, there is a partition between neutral and protonated PLCs species. In this direction, and as a first step, we have worked with three concentration corresponding to pH 7.4.

The studied concentrations range between $\sim$1:10 to 1:4 were calculated through the Eq. (1). Nevertheless, the rigidity of the used model do not allow the protonation/deprotonation processes during the simulation run.

The behavior of PLCs at physiological pH was found essentially as a combination of high and low pH: we found that all neutral PLC molecules rapidly diffuse into the hydrophobic region of the vesicle adopting an asymmetric bimodal density distribution. With concentration, the peaks position remain the same, however increase in concentration per lipid, especially on the external monolayer. By the other hand, protonated PLC are found to partition between the external monolayer and the water phase. Most of protonated drug present a great exchange between the vesicle and water phase (attaching/detaching cycles). No major difference was found in the studied concentration range. At higher simulations we observed that the increase of neutral species slightly precludes the protonated species to enter. In this study we have compared the physiological pH conditions studies with the high and low pH published before.

As a final remark, we would like to mention that molecular dynamics simulations are a very powerful tool to investigate different aspects of the encapsulation/liberation processes regarding the development/understanding the drug delivery systems at the nanoscale.

Acknowledgment: Mónica Pickholz and María Florencia Martini thanks CONICET, ANPCyT and UBACyT for financial support.

References and Notes

1. J. Calatayud and A. González, History of the development and evolution of local anesthesia since the coca leaf. *Anesthesiology* 98, 1503 **(2003)**.
2. C. Cereda, G. Brunetto, D. de Araujo, and E. de Paula, Liposomal formulations of prilocaine, lidocaine and mepivacaine prolong analgesic duration. *Canadian Journal of Anesthesia* 53, 1092 **(2006)**.
3. E. de Paula, C. Cereda, G. Tofoli, M. Franz-Montan, L. Fraceto, and D. R. de Araujo, Drug delivery systems for local anesthetics. *Recent Patents on Drug Delivery and Formulation* 4, 23 **(2010)**.
4. T. P. Herringson and J. G. Altin, Increasing the antitumor efficacy of doxorubicin-loaded liposomes with peptides anchored via a chelator lipid. *Journal of Drug Targeting* 19, 681 **(2011)**.
5. S. M. Rudramurthy, M. Jatana, R. Singh, and A. Chakrabarti, *In vitro* antifungal activity of Indian liposomal amphotericin B against clinical isolates of emerging species of yeast and moulds, and its comparison with amphotericin B deoxycholate, voriconazole, itraconazole and fluconazole. *Mycoses* doi:10.1111/j.1439-0507.2012.02197.x. **(2012)**, in press.
6. L. Lajavardi, S. Camelo, F. Agnely, W. Luo, B. Goldenberg, M.-C. Naud, F. Behar-Cohen, Y. de Kozak, and A. Bochot, New formulation of vasoactive intestinal peptide using liposomes in hyaluronic acid gel for uveitis. *J. Controlled Release* 139, 22 **(2009)**.
7. Z. Drulis-Kawa and A. Dorotkiewicz-Jach, Liposomes as delivery systems for antibiotics. *Int. J. Pharm.* 387, 187 **(2010)**.
8. G. Gregoriadis, Engineering liposomes for drug delivery: Progress and problems. *Trends in Biotechnology* 13, 527 **(1995)**.
9. A. Sharma and U. Sharma, Liposomes in drug delivery: Progress and limitations. *Int. J. Pharm.* 154, 123 **(1997)**.
10. A. Gesztes and M. Mezei, Topical anesthesia of the skin by liposome-encapsulated tetracaine. *Anesth. Analg.* 67, 1079 **(1988)**.
11. J. G. Boogaerts, N. D. Lafont, A. G. Declerq, C. L. Hongwen, E. T. Gravet, J. A. Bianchi, and F. J. Legros, Epidural administration of liposome-associated bupivacaine for the management of postsurgical pain: A first study. *J. Clin. Anesth.* 6, 315 **(1994)**.
12. G. J. Grant, Y. Barenholz, E. M. Bolotin, M. Bansinath, H. Turndor, B. Piskoun, and E. M. Davidson, A novel liposomal bupivacaine formulation to produce ultralong-acting analgesia. *Anesthesiol* 316, 133 **(2004)**.
13. K. E. Bertch, Handbook on Injectable Drugs, 16th edn., Pharmaceutical Press, London **(2011)**, Vol. 80, pp. 1008–9.
14. Y. Canos-Rius, N. Martan-Biosca, S. Sagrado, R. Villanueva-Camaatas, and M. Medina-Hernandez, Experimental and theoretical investigation of the micellar-assisted solubilization of ibuprofen in aqueous media. *European Journal of Medicinal Chemistry* 40, 215 **(2005)**.
15. E. de Paula, S. Schreier, H. Jarrell, and L. Fraceto, Experimental and theoretical investigation of the micellar-assisted solubilization of ibuprofen in aqueous media. *Biophys. Chem.* 132, 47 **(2008)**.
16. L. Cabeça, M. Pickholz, E. de Paula, and A. J. Marsaioli, Liposome-prilocaine interaction mapping evaluated through STD NMR and molecular dynamics simulations. *J. Phys. Chem. B* 113, 2365 **(2009)**.
17. L. Fraceto, A. Spisni, S. Schreier, and E. de Paula, Differential effects of uncharged aminoamide local anesthetics on phospholipid bilayers, as monitored by 1H-NMR measurements. *Biophys. Chem.* 115, 11 **(2005)**.
18. M. Pasenkiewicz-Gierula, T. Róg, J. Grochowski, P. Serda, R. Czarnecki, T. Librowski, and S. Lochy'nski, Effects of a carane derivative local anesthetic on a phospholipid bilayer studied by molecular dynamics simulation. *Biophys. J.* 85, 1248 **(2003)**.
19. C.-J. Holgberg, A. Maliniak, and A. Lyubartsev, Preferential location of lidocaine and etidocaine in lecithin bilayers as determined by EPR, fluorescence and 2H NMR. *Biophys. Chem.* 125, 416 **(2007)**.
20. M. Pickholz, L. Fraceto, and E. de Paula, Distribution of neutral prilocaine in a phospholipid bilayer: Insights from molecular dynamics simulations. *Int. J. Quantum Chem.* 108, 2386 **(2008)**.
21. E. Prates, P. Souza, M. Pickholz, and M. Skaf, CHARMM-based parameterization of neutral articaines—A widely used local anesthetic. *Int. J. Quantum Chem.* 111, 1339 **(2011)**.
22. M. Pickholz and G. Giupponi, Coarse grained simulations of local anesthetics encapsulated into a liposome, *J. Phys. Chem. B* 114, 7009 **(2010)**.
23. S. Malheiros, L. Pinto, L. Gottardo, D. Yokaichiya, L. F. Fraceto, N. C. Meirelles, and E. de Paula, A new look at the hemolytic effect of local anesthetics, considering their real membrane/water partitioning at pH 7.4. *Biophys. Chem.* 110, 213 **(2004)**.
24. S. Marrink, H. Risselada, S. Yefimov, D. Tieleman, and A. de Vries, The MARTINI force field: Coarse grained model for biomolecular simulations. *J. Phys. Chem. B* 111, 7812 **(2007)**.
25. S. Marrink and A. Mark, The mechanism of vesicle fusion as revealed by molecular dynamics simulations. of small phospholipid vesicles. *JACS* 125, 15233 **(2003)**.
26. S. Marrink and A. Mark, The mechanism of vesicle fusion as revealed by molecular dynamics simulations. *JACS* 125, 11144 **(2003)**.
27. P. Kasson and V. Pande, Control of membrane fusion mechanism by lipid composition: Predictions from ensemble molecular dynamics. *PLoS Computational Biology* 3, 2228 **(2007)**.
28. S. Yefimov, E. Van Der Giessen, P. Onck, and S. Marrink, Mechanosensitive membrane channels in action. *Biophys. J.* 94, 2994 **(2008)**.
29. X. Periole, T. Huber, S.-J. Marrink, and T. Sakmar, G protein-coupled receptors self-assemble in dynamics simulations of model bilayers. *JACS* 129, 10126 **(2007)**.
30. H. Risselada and S. Marrink, Curvature effects on lipid packing and dynamics in liposomes revealed by coarse grained molecular dynamics simulations. *Phys. Chem. Chem. Phys.* 11, 2056 **(2009)**.
31. T. Ha-Duong, N. Basdevant, and D. Borgis, A polarizable water model for coarse-grained proteins simulations. *Chem. Phys. Lett*. 468, 79 **(2009)**.
32. B. Hess, C. Kutzner, D. Van Der Spoel, and E. Lindahl, GROMACS 4: Algorithms for highly efficient, load-balanced, and scalable molecular simulation. *Journal of Chemical Theory and Computation* 4, 435 **(2008)**.
33. C. Högberg and A. Lyubartsev, Effect of local anesthetic lidocaine on electrostatic properties of a lipid bilayer. *Biophysical. J.* 94, 525 **(2008)**.
34. C. Ho, S. J. Slater, and C. D. Stubbs, Hydration and order in lipid bilayers. *Biochemistry* 34, 6188 **(1995)**.

Received: 7 May 2012. Accepted: 2 August 2012.